Nonlinear Modeling of Concrete Frame Elements including Shear Effects

Serhan Guner

Synopsis: Current nonlinear modeling software for concrete frames typically employs line elements with plastic hinges defined at user-selected locations. While this is a simple and computationally efficient approach, a number of drawbacks limit its application. They include the challenges with defining the interacting shear and moment hinge curves, uncertainties with hinge locations and lengths, and difficulties in capturing the post-peak response. Two-dimensional continuum methods address these limitations, but their computational cost limits their applicability. This study presents an alternative modeling method, and associated computer software, with the objective of combining the simplicity of frame elements with the accuracy and result visualization capabilities of continuum methods. The method, developed in the last two decades, employs a distributed-plasticity, layered-section approach based on the Disturbed Stress Field Model (DSFM). The distributed-plasticity approach eliminates the need for defining plastic hinges while the DSFM enables capturing the shear, moment, and axial force interaction. The total-load and secant-stiffness formulation provides numerically stable solutions, even in the post-peak region. This paper presents an overview of the theoretical approach, unique aspects, and capabilities of this method. The validation studies undertaken for 148 experimental specimens, subjected to static (monotonic and cyclic) and dynamic (impact, blast, and seismic) load conditions, are also presented.

Keywords: blast, cracking, failure, impact, performance-based, plastic hinges, pushover, seismic, shear.

ACI member **Serhan Guner** is an Associate Professor in the Department of Civil Engineering at the University of Toledo, OH, USA. He received his PhD from the University of Toronto, ON, Canada. He is a member of the Joint ACI-ASCE Committee 447-Finite Element Analysis, 370-Blast and Impact Load Effects, and 351-Foundations for Equipment and Machinery. His research includes finite element modeling, shear effects, disturbed regions, response to extreme loads, and the development algorithms and software.

INTRODUCTION

The success of performance-based design or assessment hinges on the accurate prediction of the structural behavior from the first cracking to the complete failure. This typically entails performing either a nonlinear static pushover or dynamic time-history analysis. Commonly used nonlinear analysis software, such as SAP2000 (CSI 2016), use slender frame elements based on the lumped-plasticity approach. While this approach is simple and computationally efficient, a number of drawbacks limit its application. The first one is the challenges associated with defining the interacting moment and shear hinges, which is not a trivial task and requires a separate nonlinear sectional analysis software, such as Response (Bentz and Collins 2001). The axial force values, which typically changes at each load stage, are also required for deriving the hinge curves. Another challenge is with the determination of the hinge locations and lengths, which introduces more uncertainty into the analysis. The third major challenge is with the calculation of the post-peak response. Most analysis software uses tangent stiffness formulation in a force-based load application mode, which typically encounters numerical instability once the peak load is reached, without being able to provide the post-peak response. The accurate prediction of the post-peak response is essential when determining the ductility, sequence of nonlinear events, and the ultimate failure mode of a frame. A rapidly decaying post-peak response indicates a brittle and undesirable behavior while a long and flat (or ascending) post-peak response indicates a ductile behaviour [Fig. 1(a)]. Another challenge is the lack of details in the analysis output for the lumped-plasticity models; typically, only the hinge condition is shown with color-coded shapes [Fig. 1(b)].

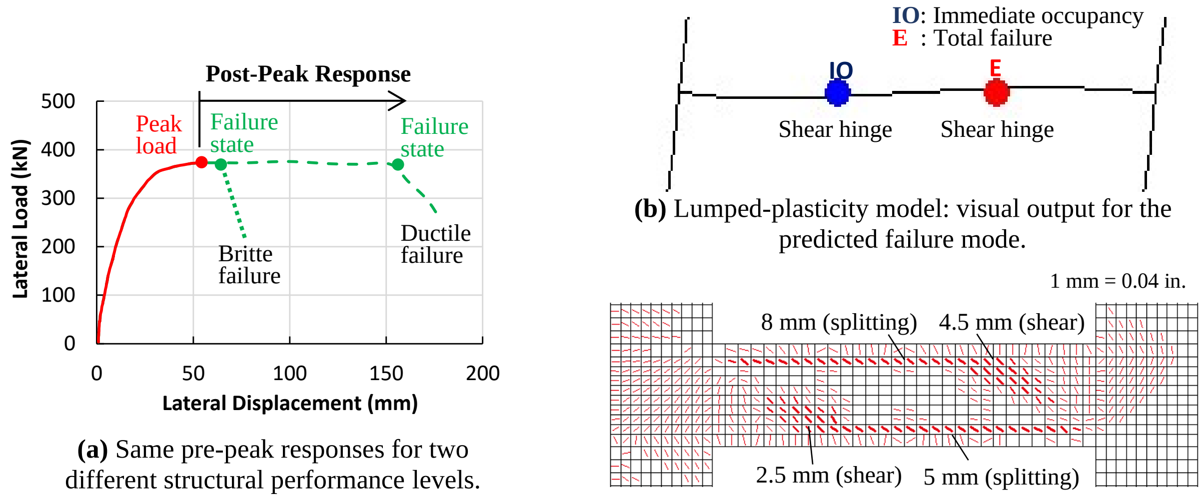

(a) Same pre-peak responses for two different structural performance levels.

(b) Lumped-plasticity model: visual output for the predicted failure mode.

(c) 2D continuum model: visual output for the predicted failure mode.

Fig. 1 – Comparison of nonlinear analysis methods for frame structures.

On the other end of the nonlinear modeling spectrum is the nonlinear continuum finite element software, such as Atena (Cervenka and Cervenka 2015) and VecTor2 (Wong et al. 2013). When used correctly and with appropriate constitutive models developed for reinforced concrete, continuum methods can capture the shear, flexural, and axial behaviors of slender and deep members, provide the post-peak response, and present the stress, strain, and cracking behavior through detailed graphics [Fig. 1(c)]. The continuum methods, however, are computationally expensive for modeling large frames and require specialized knowledge for developing valid models. The use of continuum methods is generally feasible when modeling a critical part of a frame with boundary forces obtained from a separate frame element or mixed-type analysis.

The objective of this study is to combine the simplicity of frame elements with the accuracy and result visualization capabilities of continuum elements. In pursuit of this objective, a computational modeling method and associated computer software have been developed in the last two decades through several studies. The modeling method employs a distributed-plasticity, smeared-crack approach, and material behavior models specifically developed for reinforced concrete. A layered discretization of the cross-section is adopted, which allows using frame elements but also provides detailed output for each layer. This output is used to create renderings of the frame elements and display the stress, strain, and cracking behaviour in a way similar to continuum elements. This current paper presents an overview of the theoretical approach, unique capabilities, and experimental validation studies involving 148 large-scale specimens compiled from nine previous studies.

RESEARCH SIGNIFICANCE

Performance-based design and assessment methodologies require robust and cost-effective nonlinear modeling methods to simulate the behavior of concrete frames both in the pre-and post-peak stages of the response. Capturing the shear behavior is important and remains a challenge for frame analysis software using line elements. This study describes a nonlinear analysis method and associated computer programs, developed specifically for concrete frames with the aim of capturing the shear behavior and the interaction of shear, flexural, and axial load effects. The method aims to simplify the modeling process while providing detailed analysis results comparable to continuum methods in terms of accuracy and damage visualization capabilities.

OVERVIEW OF THE FRAME ANALYSIS METHOD

The developed nonlinear analysis method uses a total-load, iterative, secant-stiffness formulation through a stiffness-based, six-degree-of-freedom frame element shown in Fig. 2(a). A fiber discretization of the cross-section is employed as illustrated in Fig. 2(b). Each concrete and longitudinal reinforcing bar layer is defined as discrete elements; the transverse reinforcement is smeared within the concrete layers, as shown in Fig. 2(c). Each layer is then analyzed based on the equilibrium, compatibility, and constitutive relationships of the Disturbed Stress Field Model (Vecchio 2000). The main sectional compatibility requirement is that ‘plane sections remain plane,’ while the sectional equilibrium requirements include balancing the axial force, shear force, and bending moment calculated by the global frame analysis. A parabolic shear strain distribution through the section depth is used in all analyses due to its ability to continue an analysis into the post-peak region. The descriptions of this and other implemented approaches may be found in Guner (2008). While the clamping stresses in the transverse direction are taken as zero, a shear protection algorithm is employed to mitigate the premature failures of D-regions. This algorithm detects the joints of frames (beam and column connection nodes), the point load application points, and the supports. It then reduces the shear force demands on these members and the members that fall in a distance of 0.7 times the section height as per the CSA A23.3 (2024) requirements. More details of this implementation may be found in Guner (2008).

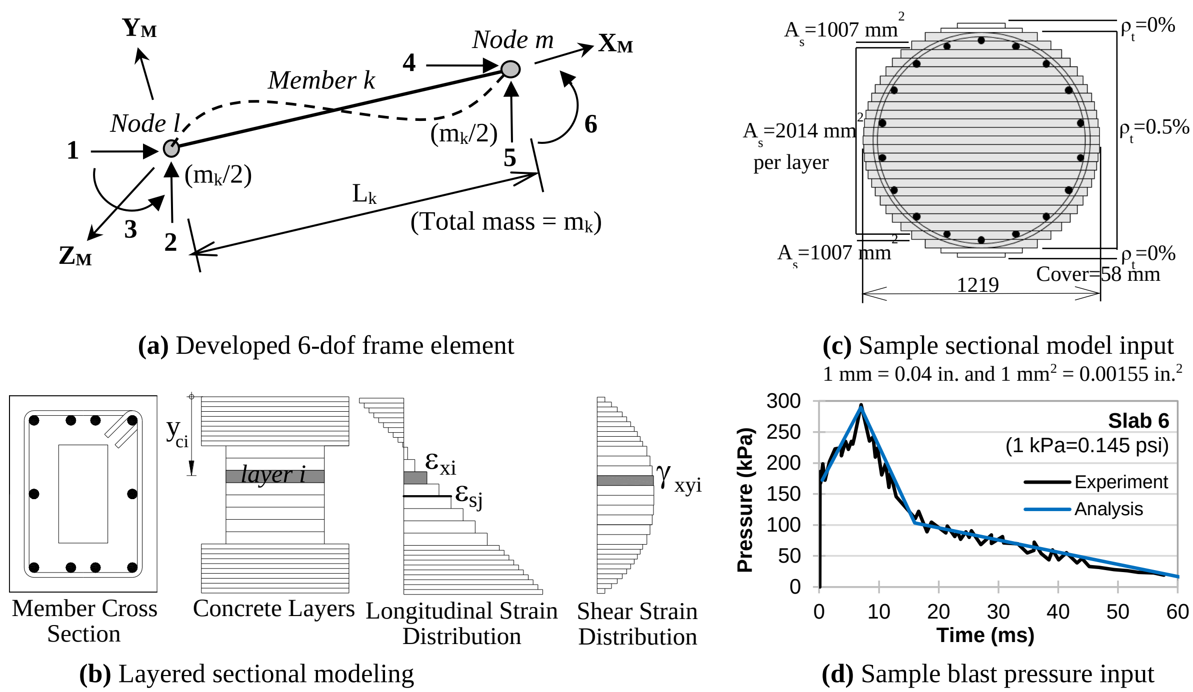

(a) Developed 6-dof frame element

(c) Sample sectional model input
1 mm = 0.04 in. and 1 mm² = 0.00155 in.²

(b) Layered sectional modeling

(d) Sample blast pressure input

Fig. 2 – Components of the frame analysis method and VecTor5.

The formulations of the method are coded into an executable computer program, VecTor5 (Guner and Vecchio 2008). To facilitate the model development and result visualization in a Windows-based graphical environment, pre- and post-processor programs were developed. Pre-processor FormWorks Plus (Blosser et al. 2016, Wong et al. 2013, Sadeghian 2012) provides modeling capabilities in a graphical environment with auto-meshing and sub-structuring facilities, while post-processor Janus (Loya et al. 2017, Chak 2013) displays the analysis results. The results include the displaced shape of the structure, crack widths, locations and propagation characteristics under increased loading, rebar and concrete stresses and strains, and failure conditions. The post-processor program is a critical component of numerical modeling process by enabling the user to understand the structural behavior, detect modeling mistakes, and effectively compare the calculated responses.

Material Constitutive Models

Concrete behavioral modeling is performed in accordance with the formulations of the DSFM (Vecchio 2000), a cracked concrete dedicated material model developed as an extension to the Modified Compression Field Theory (MCFT) (Vecchio and Collins 1986). This smeared, hybrid rotating-fixed crack analysis method considers the redistribution of internal forces that can occur due to local changes in stiffness arising from cracking or crushing of concrete or yielding of the steel reinforcement. In addition, the concrete compression softening attributed to the co-existing lateral tension, the presence of post-cracking concrete tensile stresses between crack locations, and the influences associated with variable and changing crack widths are also considered in the formulation.

While cracked concrete material modeling is principally conducted in accordance with the formulations of the DSFM, a library of advanced material behavior models for concrete, reinforcement, and their bond and interaction are used. To simplify the modeling process and permit cost-effective solutions for a given problem, one default model is recommended for each material behavior (see Table 1). These default models are found, through validation studies, to perform well for applications commonly encountered in practice. Other material models are also available and presented in Wong et al. (2013).

Table 1 – Advanced material behavior models included (default models are shown).

Material Behavior	Default Model	Material Behavior	Default Model
Compression base curve	Hognestad, Popovics or Hoshikuma et al.	Concrete hysteresis	Nonlinear w/ plastic offsets
Compression post-peak	Modified Park-Kent	Slip distortion	Walraven
Compression softening	Vecchio 1992-A	Strain rate effects	fib Model Code - Malvar
Tension stiffening	Modified Bentz 2003	Rebar hysteresis	Seckin w/ Bauschinger
Tension softening	Linear	Rebar dowel action	Tassios (Crack slip)
Confinement strength	Kupfer / Richart	Rebar buckling	RDM Model (Akkaya et al.)
Cracking criterion	Mohr-Coulomb (Stress)	Geometric nonlinearity	Considered
Crack width check	Agg/5 Max crack width	Previous loading history	Considered

The concrete hysteresis model [Fig 3(a)] uses a plastic-offset modeling approach (Vecchio 1999) following a nonlinear Ramberg-Osgood formulation. Popovics (1973) and Modified Park-Kent (Mander et al. 1988, Scott et al. 1982, Kent and Park 1971) models are adopted to establish the backbone curves for the pre- and post-peak regions. Confinement effects [Fig 3(b)] are modelled using the formulations of Kupfer et al. (1969) and Richart et al. (1928).

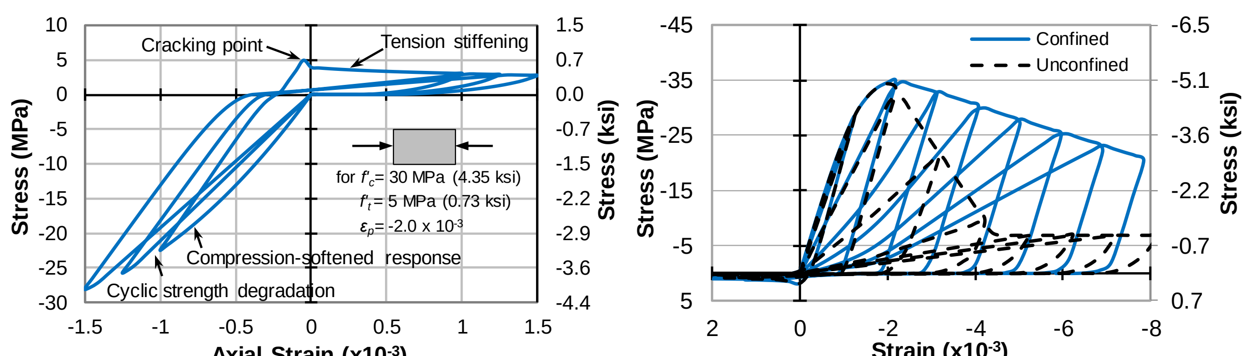

(a) Compression softening and tension stiffening effect **(b)** Confinement effects

Fig. 3 – Concrete constitutive models.

The reinforcing steel hysteresis response is based on the Seckin model with the Bauschinger effect (Seckin 1981) in tension [Fig 4(a)], and the RDM model (Akkaya et al. 2019) in compression [Fig 4(b)]. The RDM model accounts for the interactions between lateral ties and longitudinal bars and simulates the compressive stress-strain response of reinforcing bars, including the onset of inelastic buckling and subsequent degradation in the post-buckling regime. Formulation details and the open-access code of the RDM model may be obtained from Akkaya et al. (2019).

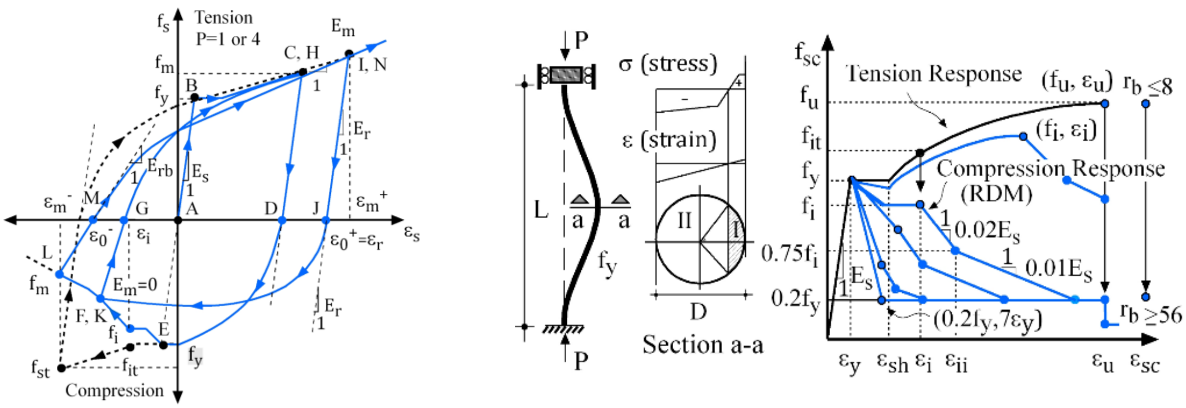

(a) Reinforcing bar hysteresis model **(b)** Backbone curves for buckling parameter r_b ranging from 8 to 56

Fig. 4 – Reinforcing bar constitutive model (Akkaya et al. 2019, Seckin 1981).

Solution Algorithm

A total-load secant-stiffness formulation is used to improve the convergence and provide the post-peak response, addressing a major limitation of incremental load, tangent stiffness formulations adopted by most nonlinear frame analysis software. A shear-strain-based analysis is used to calculate the longitudinal stress σ_x and shear stress τ_{xy} of each concrete layer in an iterative manner until the total strain in the transverse direction ε_y converges. The resultant sectional forces are obtained by superposition the concrete and reinforcement responses. The calculated forces are returned to the global frame analysis algorithm where they are checked with the member forces obtained from the global frame analysis to determine the unbalanced forces. The objective of the global frame analysis is to reduce all unbalanced forces to zero before proceeding to a new load or time stage. More details on the calculation process are provided in Guner and Vecchio (2010a).

Cyclic Load Conditions

A plastic offset formulation is used to consider the concrete and reinforcement plastic strains as a part of the total strains. In this implementation, the plastic offset strains incurred by the concrete under load reversals are defined and retained. Since a rotating crack approach is used, the principal strain directions are free to rotate; therefore, the plastic offset strains must be defined with respect to the local x- and y-axes so that the previous damage does not rotate with the rotation of the principal strain directions. For this purpose, an incremental formulation is employed. In this calculation, previously stored concrete plastic offset strains $\varepsilon_{cx}{}^p$, $\varepsilon_{cy}{}^p$, $\gamma_{cxy}{}^p$ are transformed into principal concrete plastic offset strains $\varepsilon_{c1}{}^p$ and $\varepsilon_{c2}{}^p$. The elastic strain components, not the total strains, are used to determine the current orientation of the stress field θ. At the same time, the instantaneous concrete plastic offset strains are calculated based on the selected concrete hysteresis model. If the instantaneous plastic offset strains exceed the previously stored plastic offset strains, incremental plastic offset strains are generated. More details on these formulations are provided in Guner and Vecchio (2011).

Dynamic Load Conditions

An explicit three-parameter time-step integration method is developed for the solution of the dynamic equation of motion (Eq. 1) based on a total-load secant-stiffness formulation. One of the three numerical analysis methods may be employed by substituting: $\gamma = 1/2$, $\beta = 1/4$ and $\theta = 1$ for Newmark's average acceleration method; $\gamma = 1/2$, $\beta = 1/6$ and $\theta = 1$ for Newmark's linear acceleration method; and $\gamma = 1/2$, $\beta = 1/6$ and $\theta = 1.42$ for Wilson's theta method. The main equations of the solution are provided below. More details may be found in Guner and Vecchio (2012).

$$\left[\left[k_{stat}\right]+\left[k_{dyn}\right]\right]\times\left\{u_1\right\}=\left\{p_{stat}\right\}+\left\{p_{dyn}\right\} \quad (1)$$

$$\left[k_{dyn}\right]=\frac{[m]+[c]\times\gamma\times(\theta\times\Delta t)}{\beta\times(\theta\times\Delta t)^2} \tag{2}$$

$$\left\{p_{dyn}\right\}=\left\{p_1 *\right\}+\frac{[m]+[c]\times\gamma\times(\theta\times\Delta t)}{\beta}\times\left[\frac{\{u_0\}}{(\theta\times\Delta t)^2}+\frac{\{\dot{u}_0\}}{(\theta\times\Delta t)}+\frac{\{\ddot{u}_0\}}{2}\right]-[c]\times\left\{\{\dot{u}_0\}+(\theta\times\Delta t)\times\{\ddot{u}_0\}\right\}-[m]\times\{\ddot{u}_0\} \tag{3}$$

Strain Rates

When subjected to high rates of loading, concrete and reinforcing steel materials exhibit increased strength. This strength gain is considered through a dynamic increase factor (DIF) approach, in which the strain rate values for each concrete and steel layer are determined from the slope of the strain-time response. The corresponding DIFs are calculated and applied to the static material properties. As the default models, the *fib* Model Code (fib 2010) and Malvar (1998) formulations are used for concrete, and reinforcement, respectively (Fig. 5).

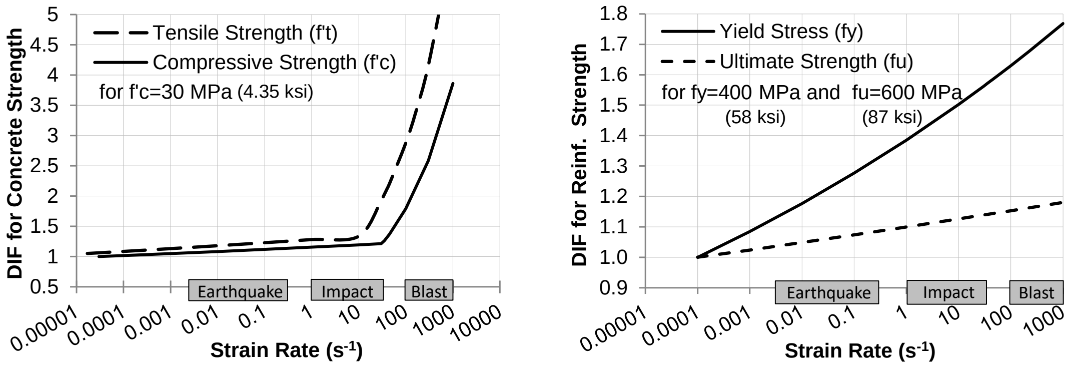

Fig. 5 – Strain rate - dynamic increase factor (DIF) models for concrete and reinforcing steel.

Structural Damping

The actual damping associated with the computed responses is primarily accounted for by the steel reinforcement and cracked concrete material hysteresis models. This eliminates the need to define an estimated damping ratio which is dependent on the specific frame configuration and damage mode. In addition, supplementary damping may be defined, using one of the two formulations implemented, to improve the damping response for low damage or primarily linear-elastic response cases. The first formulation implemented employs Rayleigh damping (Rayleigh 1877), in which two damping ratios can be assigned to two vibration modes. The second formulation incorporated employs 'alternative damping' and is useful when the exact specification of damping ratios to more than two vibration modes is needed. Details of both formulations can be found in Clough and Penzien (1993).

Deep Beam Modeling

Deep beams are characterized by small shear span-to-depth ratios. They carry shear by direct compression between the loading and support points, which is known as the strut or arch action. The 'plane-sections-remain-plane' hypothesis does not apply to deep beams; therefore, deep beams cannot be accurately analyzed by most nonlinear frame analysis methods. To provide an analysis capability where slender and deep beam elements may be used in a frame model, a mixed-type analysis framework is developed and implemented in VecTor5. The framework integrates slender beam elements (as discussed in above sections) with equally simple deep beam elements that can account for the strut action. The deep beam element incorporated was formulated by Liu and Mihaylov (2018) based on a three-parameter kinematic theory for continuous deep beams (Mihaylov et al. 2015). This element models the entire nonlinear shear response of deep shear spans, from initial high stiffnesses to the post-peak response, which provides the structure with the ability to redistribute forces and survive overloading. To solve the nonlinear equations of the deep beam element, a secant stiffness approach is used to provide compatibility with the existing slender beam elements. Based on this, the stiffnesses of the three springs of the element are obtained as $k_1=M_1/\theta_1$, $k_2=M_2/\theta_2$ and $k_3=V/\Delta_c$ (Fig. 6). More details on the formulation and application of this deep beam element may be found in Liu et al. (2019).

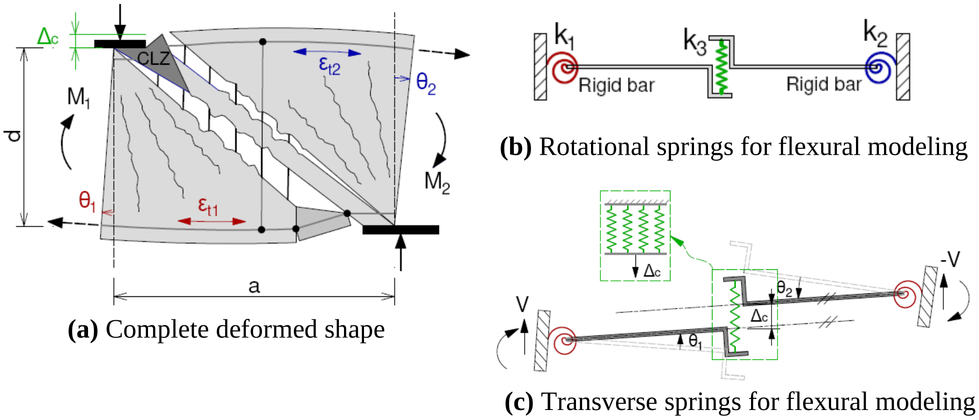

(a) Complete deformed shape

(b) Rotational springs for flexural modeling

(c) Transverse springs for flexural modeling

Fig. 6 – Three-parameter kinematic model adopted (Liu and Mihaylov 2018, Liu et al. 2019).

Beam-Column Joint Modeling

In the analysis of concrete frames subjected to seismic loading, beam-column joints are commonly assumed rigid or semi-rigid. This assumption implies that the joint core remains elastic and deforms as a rigid body throughout the lateral loading event, even if the beams and columns undergo significant deformation and sustain severe damage. The experimental studies on the seismic performance of non-ductile beam-column joints conducted by Walker (2001) have demonstrated that joint deformations due to shear cracking and bond slip are major contributors to story drifts. To provide an analysis capability for modeling the nonlinear behavior of frame joints, a two-dimensional, thirteen degree-of-freedom component model is implemented to simulate the inelastic behavior of beam-column joints. This element consists of three components: (1) eight zero-length bar slip springs to simulate the strength and stiffness loss in the bond between the concrete and reinforcing bars; (2) four interface shear springs to simulate the shear transfer from beams and columns to the joint; and (3) a panel element to simulate shear deformations in the joint region (Fig. 7). More details on the formulation and application of this element may be found in Pan et al. (2017).

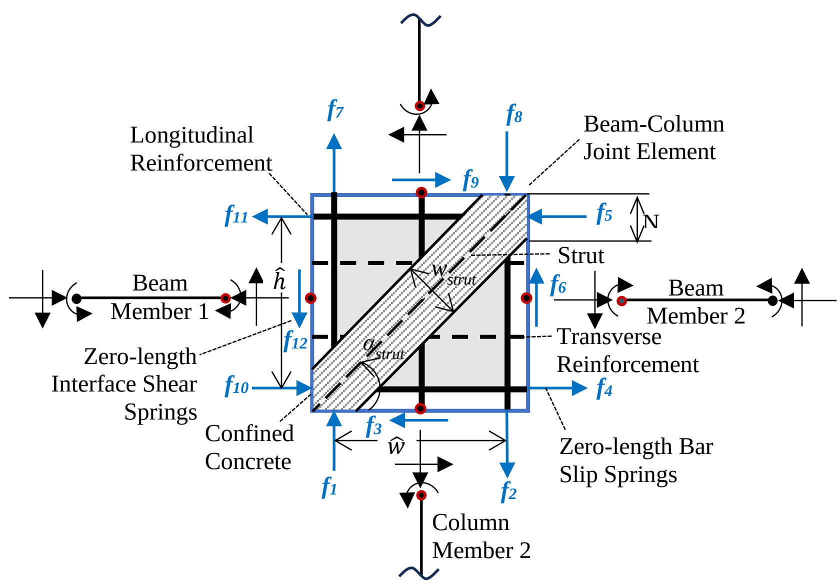

Fig. 7 – Beam-column joint model adopted (Pan et al. 2017).

Model Creation, Analysis, and Result Acquisition

Numerical models are created using the pre-processor program FormWorks Plus (Blosser et al. 2016, Wong et al. 2013, Sadeghian 2012) which provides modeling capabilities in a Windows-based graphical environment with auto-meshing and sub-structuring facilities. The analyses are conducted using the computer program VecTor5. The analysis results are visualized using the post-processor program Janus (Loya et al. 2017, Chak 2013) which displays the displaced shape of the structure, crack widths, locations and propagation characteristics under increased loading, rebar and concrete stresses and strains, and failure conditions. The post-processor program is a critical component of numerical modeling process by enabling the user to understand the structural behavior, detect modeling mistakes, and effectively compare the calculated responses.

VALIDATION STUDIES

The developed method has been validated with 148 large-scale experimental tests that include a large range of geometry, material properties, reinforcement details, and loading conditions. Most specimens are selected to exhibit shear-critical behavior to validate the shear modeling capabilities. The calculated responses are compared with the experimental ones in terms of strength, stiffness, crack widths and patterns, reinforcement stresses and strains, concrete stresses and strains, and failure modes and displacements. The following sections present one sample validation study for each load condition (monotonic, cyclic, impact, blast, and seismic) and special element type developed (deep beam and beam-column joint elements).

Static Load Conditions

Monotonic loading

Monotonic loading refers to quasi-static load applications in increasing magnitude. The analysis performed under this loading is commonly referred to as the pushover analysis. To validate the developed method for monotonic load cases, 38 large-scale experimental specimens, tested by eight research teams, were modelled. The associated experimental publications include Vecchio and Shim (2004), Angelakos et al. (2001), Vecchio and Emara (1992), Doung et al. (2007), Vecchio and Bolopoulou (1990), Wu et al. (2008), Yavari et al. (2013) and Xue at al. (2011). The specimen selection was made based on the availability of the published studies with sufficient details suitable for numerical modeling. In addition, the specimens with shear-critical behavior were given priority to be able to validate the shear modeling capabilities. 68% of the selected specimens (26 of 38) exhibited shear-critical behavior in the experimental tests.

As an example, validation studies conducted for a shear-critical frame is presented in Fig. 8. The frame has a height of 4,600 mm, including the base beam. The beam and column cross sections are 300 mm (11.8 in.) by 400 mm (15.7 in.). The frame was subjected to 420 kN (94.4 kips) column axial loads and a monotonically increasing lateral displacement. More details on this experimental program may be found in Doung et al. (2007). The analysis model was created with the help of the pre-processor program FormWorks+ [Fig. 8(a)]. Six member types, each with 40 concrete layers, were used to model the beam, column, and base cross sections. An additional six member types were used to represent the beam-column joints. More details on this numerical model may be found in Guner and Vecchio (2010b).

The developed method was able to calculate the strength, ductility, initial stiffness, and the softening in the stiffness accurately [Fig. 8(b)]. The damage mode of the frame was experimentally classified as flexure-shear with significant shear damage at the north end of the first story beam, accompanied by flexural cracking and reinforcement yielding [Fig 8(c)]. The developed method calculates and outputs analysis results for each concrete and reinforcing bar layer, which are read by the post-processor program Janus and presented graphically [Fig. 8(d)]. This provides a unique capability where the modeling is conducted with the simplicity of frame elements, but the results are obtained as if a 2D finite element analysis was undertaken. In contrast, the results obtained from the frame elements of SAP2000 are shown in Fig. 8(e), where the red dot represents failure. The model with user defined hinges predicted beam shear failure but no flexural yielding. The use of default hinges resulted in a highly inaccurate response prediction, as shown in Fig. 8(b). More details on these models may be found in Guner (2008).

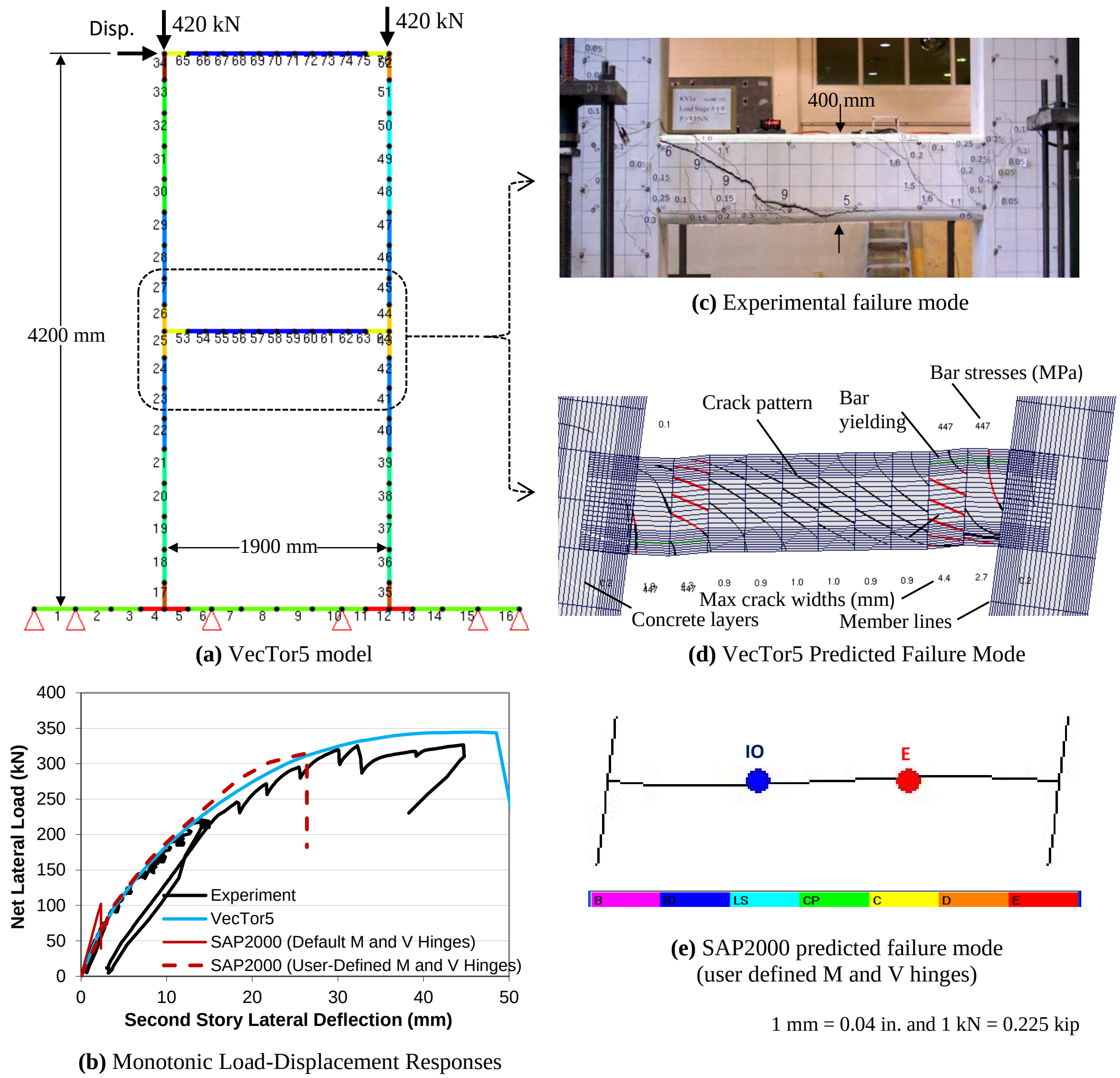

(a) VecTor5 model

(b) Monotonic Load-Displacement Responses

(c) Experimental failure mode

(d) VecTor5 Predicted Failure Mode

(e) SAP2000 predicted failure mode (user defined M and V hinges)

1 mm = 0.04 in. and 1 kN = 0.225 kip

Fig. 8 – Sample analysis model and results for a shear-critical frame.

Cyclic Loading

Cyclic loading refers to quasi-static application of loading and unloading cycles. In experimental studies, well-defined cycles with an amplitude increase rule are commonly used while arbitrary load cycles are applied during earthquake events or shake table tests. The developed method is formulated to allow both cases of cyclic loads. To validate the developed method for cyclic load cases, 22 large-scale experimental specimens, tested by four research teams, were modelled. The associated experimental publications include Doung et al. (2007), Seckin (1981), Shiohara and Kusuhara (2006), and Oesterle et al. (1976).

As an example, validation studies conducted for a shear wall are presented in Fig. 9. The wall had a height of 4,573 mm (180 in.), measured from the top of the base beam, and a cross section of 1910 (75 in.) by 102 mm (4 in.) with a barbell size of 305 by 305 mm (12 in.). The wall was subjected to 1,200 kN (270 kips) axial load and a monotonically increasing lateral load. More details on this experiment program may be found in Oesterle et al. (1976). A simple analysis model is created with the help of the pre-processor program FormWorks+ [Fig. 9(a)]. Two member types, each with 96 concrete layers, are used to model the wall and top loading beam. The base beam is represented by a fixed support. More details on this numerical model may be found in Guner and Vecchio (2011).

The damage mode of Wall B7 was reported to include flexural mechanisms with significant web crushing (Palermo and Vecchio 2004). Similar results were obtained numerically. The analysis results indicate a flexural crack width of

8.7 mm (0.34 in.) with 76.5 x 10^{-3} longitudinal reinforcement straining and crushing of the web concrete for Member 1 [Fig. 9(b)]. In addition, the overall behavior of the wall, including its strength, is predicted accurately [Fig. 9(c)]. The total energy dissipated by the wall under load cycles was calculated as 576.6 kNm (425.3 kips-ft) which compares well with the experimental value of 501.3 kNm (369.7 kips-ft). The displacement ductility was calculated as 13.6 as compared to the experimental value of 14.3. Considering the simplicity of modeling with line elements, the obtained results provide a good value for the accuracy and extent of details.

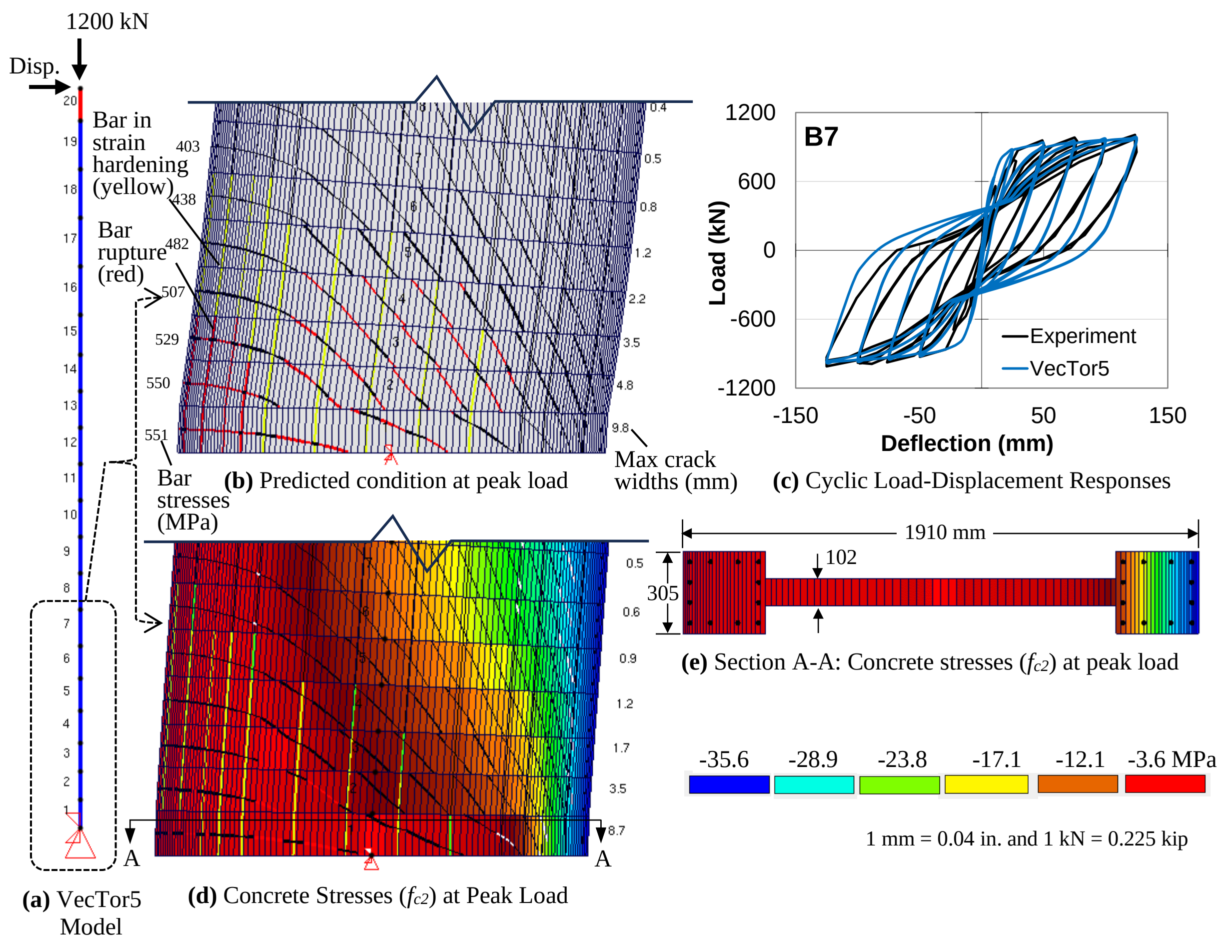

Fig. 9 – Sample shear wall analysis model and results.

Deep Beam Modeling

To validate the deep beam analysis capabilities, 17 simply supported deep beams, one continuous deep beam, and one large frame structure, tested by three research teams, were modeled. The associated experimental publications include Tanimura and Sato (2005), Salamy et al. (2005) and Mihaylov et al. (2010). All beams were shear-critical and modelled with both VecTor5 and a continuum finite element method (FEM).

As an example, the modeling studies conducted for two deep beams, tested by Tanimura and Sato (2005) and Salamy et al. (2005), are presented in Fig. 10. The beams had the shear span-depth ratios of 0.5 and 1.5, the effective depths of 400 and 1200 mm (15.8 and 47.2 in.), the longitudinal reinforcement ratios of 2.14% and 1.99%, and the concrete compressive strengths of 23.2 and 27 MPa (3.37 and 3.92 ksi), respectively. They did not contain any shear reinforcement. Other details on the experimental program may be found in the references cited above.

The frame model was created for one-half of the specimens benefiting from the symmetry [Fig. 10(a)]. A slender element, shown as Member 2, is used for the pure bending region while a deep element, shown as Member 1, is used for the shear span to demonstrate the compatibility of these two element types in the same analysis model. The 2D finite element models consist of approximately 250 elements including quadrilaterals for concrete and discrete truss bars for the longitudinal reinforcement [Fig 10(b)]. Both beams exhibited shear-critical behavior in the experiments [Fig 10(c)]. The crack pattern calculated by VecTor5 is presented in Fig 10(d). Due to the smeared crack approach used, the cracks are distributed across the element, but the large width of the shear crack hints the possibility of a few major cracks. The load-deflection responses obtained from the frame (VecTor5) and 2D (nonlinear continuum) models are presented in Fig. 10(e). Overall, both approaches capture the pre-peak response and produce satisfactory strength predictions within ±10% – well inside the margins of error expected when analyzing shear-critical concrete members. While the frame approach (VecTor5) is slightly more conservative than the 2-D (FEM) approach, the frame approach produced better results in the post-peak regime. The post-peak response has a special importance when evaluating the ductility and resilience of a member under extreme loads. When considering the simple modeling and fast analysis characteristics of the developed frame modeling approach, the results obtained present a good value.

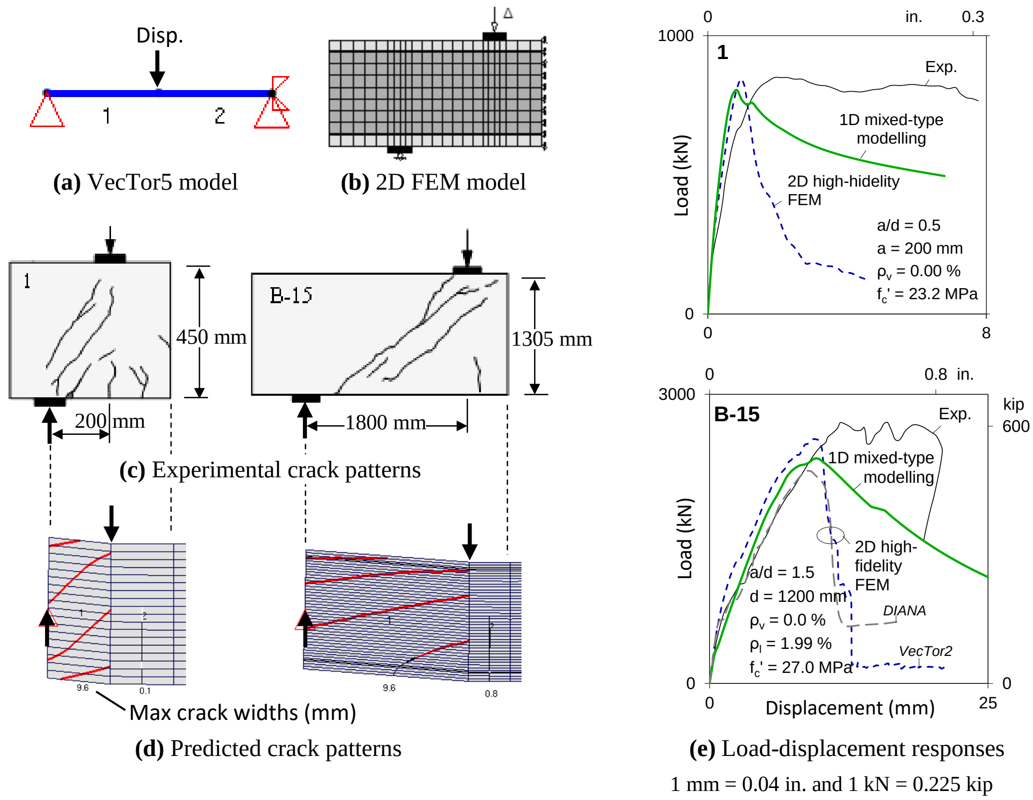

Fig. 10 – Sample deep beam analysis models and results.

Beam-Column Joint Modeling

To validate the joint modeling capabilities, nine interior beam-column subassemblies, tested by four research groups, were modeled. The associated experimental publications include Shiohara and Kusuhara (2006), Park and Dai (1988), Noguchi and Kashiwazaki (1992), and Attaalla and Agbabian (2004).The specimens considered cover various material properties, reinforcement ratios, and failure mechanisms. The specimens were modelled using the new joint element.

As an example, Specimen SHC2, tested by Attaalla and Agbabian (2004), is presented in Fig. 11. This specimen had only two transverse ties in the joint core. The frame model included 32 elements [Fig. 11(a)]. The experimental peak load was 16.7 kN (3.75 kips) at a displacement of 100 mm (4 in.). The longitudinal reinforcement of the beams yielded at the joint interface at a displacement of 28 mm (1.10 in.). The maximum shear stress of the joint panel was 7.2 MPa (1.04 ksi) with the corresponding maximum shear strain of 8.7 x 10^{-3}. The analysis predicted the behavior of the subassembly well [Fig. 11(b)]. The peak load was predicted as 18.4 kN (4.14 kips) at a displacement of 86 mm (3.4 in.). The maximum shear stress of 5.8 MPa (0.84 ksi) was reached at a displacement of 82 mm (3.2 in.) with the corresponding shear strain of 12.2 x10^{-3}. The predicted failure mechanism was the yielding of the beam followed by the failure of the joint [Fig 11(c)], matching well with the experimental observations [Fig 11(d)]. The load-displacement response obtained from the frame model with semi-rigid joints is also shown in Fig. 11(b). This approach overestimated the peak load capacity of the joint by 30%, leading to unconservative response predictions. The stiffness of the frame is also overestimated owning to the omission of joint shear deformations. In a frame with several joints, these overestimations may accumulate, leading to highly inaccurate global response predictions.

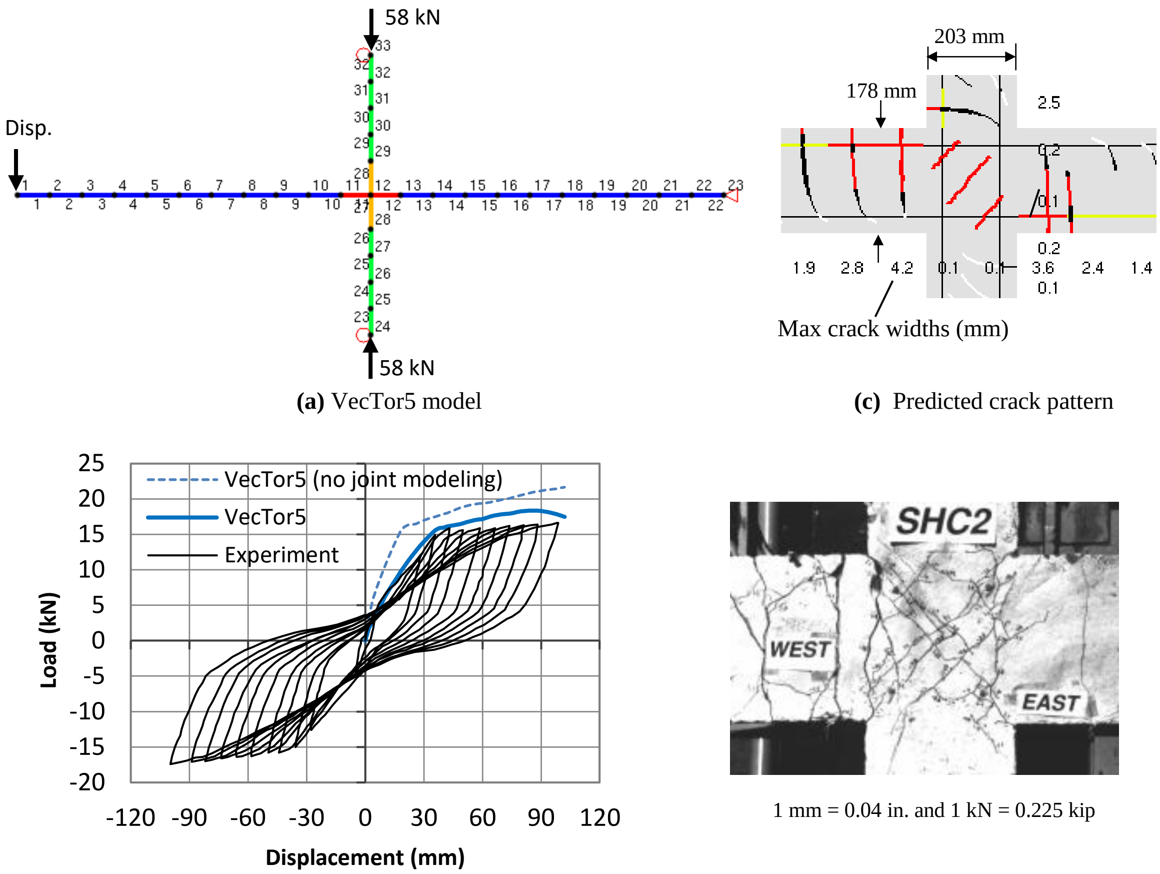

(a) VecTor5 model

(c) Predicted crack pattern

(b) Load-displacement response

1 mm = 0.04 in. and 1 kN = 0.225 kip

(d) Experimental crack pattern

Fig. 11 – Sample beam-column joint analysis model and results.

Summary of Results

The peak load capacities obtained from all static load analyses are presented in Table 2 in comparison with the experimental results. Considering all 86 monotonically loaded beam, frame, shear wall, deep beam and beam-column joint specimens, a mean of 1.01 and a coefficient of variation of 11.3% are obtained for the calculated-to-experimental peak load ratios. Considering the challenges involved in capturing the shear-critical behavior and the simplicity of the method used, these values may be regarded as highly satisfactory. The results obtained from a sophisticated continuum FEM for deep beams are also presented. The closeness of the mean and coefficient of variation values further demonstrates the value obtained from the developed method. In addition, the stiffnesses, cracking behavior, failure modes, failure displacements, and post-peak responses are also captured well. More details on the modeling studies undertaken for these specimens may be found in the references cited in Table 2. These specimens, most of which are shear-critical, are highly suitable for use as benchmark specimens. The readers are encouraged to model some of these specimens to gauge the accuracy of the modeling method and software that they use.

Dynamic Load Conditions

Dynamic load conditions considered include impact, blast, and seismic loads. Unlike quasi-static load analyses, dynamic load analyses do not use imposed forces or displacements as a mechanism to load the structure to failure. Impact loads are defined through an impact force history. If the acceleration of the impacting mass at the point of impact is known, the impacting mass and acceleration may be used as a more convenient, and more reliable, option for the impact load input. Blast loads may be defined through a blast pressure history [see Fig. 2(d) for a sample]. These histories may be obtained from the governing blast design codes or specifications. For experimental validation studies, which are typically conducted in well-controlled shock tube facilities, the measured shock wave pressure histories are used as the loading input. Seismic loads are defined through a ground accelerations data file, which includes time and acceleration data points. The acceleration data, typically with thousands of data points, may be obtained from online resources for past earthquakes. Synthetic ground motions or acceleration data can also be created.

Impact and blast loads are very short duration events measured in milli-seconds (ms); these analyses typically run in a short period of time. Earthquake events may last over 60 seconds and typically require much longer analysis execution times even when using fast analysis methods.

Table 2 – Comparison of the calculated peak loads with experimental values for static load conditions.

Monotonic Loading			Peak Load (kN)		
		Specimen	VT5	Exp.	VT5/Exp
1	**Beams** (Guner and Vecchio 2010b)	VS-OA1	331	331	1.00
2		VS-OA2	376	320	1.17
3		VS-OA3	420	385	1.09
4		VS-A1	487	459	1.06
5		VS-A2	481	439	1.10
6		VS-A3	430	420	1.02
7		VS-B1	459	434	1.06
8		VS-B2	371	365	1.02
9		VS-B3	351	342	1.03
10		VS-C1	272	282	0.96
11		VS-C2	331	290	1.14
12		VS-C3	268	265	1.01
13		DB120	387	358	1.08
14		DB130	431	370	1.16
15		DB140	412	360	1.14
16		DB165	454	370	1.23
17		DB180	450	344	1.31
18		DB230	575	514	1.12
19		DB0.53	304	330	0.92
20		DB0.53M	539	526	1.02
21		DB120M	628	564	1.11
22		DB140M	664	554	1.20
23		DB165M	660	904	0.73
24		DB180M	666	790	0.84
25	**Frames** (Guner and Vecchio 2010b, Peng and Guner 2018)	Vecchio & Emara	324	322	1.01
26		Duong et al.	349	325	1.07
27		Vecchio & Bolopoulou	570	519	1.10
28		Ghannoum	105	122	0.86
29		Wu et al.	107	124	0.86
30		MCFS	195	220	0.89
31		HCFS	205	218	0.94
32		Xue et al.	249	227	1.10
33	**Walls** (Guner and Vecchio 2010b)	SW21	120	128	0.94
34		SW22	139	150	0.93
35		SW23	151	180	0.84
36		SW24	119	120	0.99
37		SW25	147	150	0.98
38		SW26	115	123	0.93
				Mean	**1.03**
				CV	**11.7%**

Cyclic Loading			Peak Load (kN)		
		Spec.	VT5	Exp.	VT5/Exp
1	**Frame**	Duong+	348	327	1.06
2		Duong-	-311	-304	1.03
3	**Beam-Column Joints**	SP6+	121	117	1.04
4		SP6-	-75	-83	0.91
5		SP7+	122	111	1.1
6		SP7-	-77	-86	0.9
7		A2+	74	79	0.93
8		A2-	-74	-76	0.97
9		A3+	173	178	0.97
10		A3-	-121	-123	0.99
11	**Shear Walls**	B1+	260	282	0.92
12		B1-	-248	-289	0.86
13		B2+	664	692	0.96
14		B2-	-631	-709	0.89
15		B7+	976	1004	0.97
16		B7-	-972	-1011	0.96
17		B8+	964	968	1.00
18		B8-	-962	-1064	0.9
19		R1+	115	121	0.95
20		R1-	-111	-120	0.92
21		F1+	844	852	0.99
22		F1-	-765	-818	0.93
(Guner and Vecchio 2011)				Mean	**0.96**
				CV	**6.0%**

Deep Beam Element		Peak Load (kN)		
	Specimen	Experm.	VT5/Exp	FEM/Exp
1	Beam 1	853	0.94	0.93
2	Beam 2	821	1.00	0.93
3	Beam 3	833	0.98	0.92
4	Beam 4	869	0.93	0.87
5	Beam 5	632	0.88	1.06
6	Beam 6	731	0.81	1.00
7	Beam 7	750	0.83	1.03
8	Beam 8	804	0.81	1.10
9	Beam 9	284	1.25	1.28
10	Beam 10	464	0.88	1.06
11	Beam 11	491	1.01	1.19
12	Beam 12	570	1.01	1.09
13	B-10-2	357	0.71	0.93
14	B-13-2	1128	0.91	1.00
15	B17	2607	0.92	1.02
16	B15	2695	0.86	0.94
17	B18	4419	1.05	1.12
(Liu et al. 2019)		Mean	**0.93**	**1.03**
		CV	**12.6%**	**10.2%**

Joint Element			Peak load	
	Specimen	Analy.	Exp.	Ratio
1	A1	94.0	126.6	0.74
2	D1	112.7	133.9	0.84
3	U1	94.7	80.0	1.18
4	U2	132.7	111.0	1.20
5	OKJ2	265.6	237.0	1.12
6	OKJ6		214.0	1.23
7	SHC1	16.4	16.0	1.02
8	SHC2	18.4	16.7	1.10
9	SOC3	15.7	16.0	0.94
(Pan et al. 2017)			Mean	**1.04**
			CV	**15.4%**

	Cummulative
Number of specimens	86
VT5/Exp **Mean**	**1.01**
VT5/Exp **CV**	**11.3%**

1 kN = 0.225 kip

To validate the developed method for dynamic load conditions, 62 large-scale experimental specimens, tested by seven research groups, were modelled. The associated experimental publications include Saatci and Vecchio (2009a,b), Thiagarajan and Johnson (2014), Robert and Johnson (2009), Jacques (2011), Dunkman et al. (2009), Hachem et al. (2003), and Elwood and Moehle (2003). The specimen section was made based on the availability of well-detailed published studies suitable for numerical modeling. In addition, the specimens with shear-critical behavior were given priority to be able to validate the shear modeling capabilities.

As an example, the impact load validation studies conducted for a large-scale beam, tested by Saatci and Vecchio (2009a,b) at the University of Toronto, are presented in Fig. 12. Four pairs of beams were tested subjected to free-falling weights, with an impact velocity of 8.0 m/s (26.2 ft/s). The beams were subjected to multiple testing, providing a total number of 20 impact tests. The main variable was the amount of the transverse reinforcement, ranging from 0.0 to 0.3%. The concrete strengths also varied slightly, ranging from 44.7 MPa to 50.1 MPa (6.5 to 7.3 ksi). The experimental program was comprised of Beams SS0 to SS3, where the numbers from 0 to 3 denote the transverse reinforcement ratios from 0 to 0.3%. The a-series and b-series beams were identical in all aspects except the impact loading protocol employed.

The frame model, including 11 elements, was created for one-half of the beam benefiting from the symmetry. The sectional model uses 32 concrete layers in a symmetrical layout. A special modeling technique is used to model the impacting mass, where an impact transfer element (i.e., Member 11) is created with a very high stiffness to create a hard impact, and a linear-elastic compression-only behavior to permit the separation of the drop-weight from the beam after an impact. The impacting load is simulated by assigning an initial velocity of 8.0 m/s (26.2 ft/s) to the mass defined at Node 12. The Wilson's theta method, with no additional viscous damping, and a time step length of 0.01 ms, was used in all analyses.

The results were investigated in terms of the midspan displacement and support reaction responses, member deformations, concrete crack widths, reinforcement stresses and strains, the failure modes, and the failure displacements through the post-processor program Janus [Fig. 12(b) and 12(c)]. For Beam SS1, the calculated crack widths, damage levels, and failure modes, show good correlation with the experimental observations [Fig. 12(a) and (b)]. The shear and moment diagrams are also calculated and displayed for every time step [Fig. 12(c)]. The peak displacements of the beams are calculated accurately [Fig. 12(d)]. Considering the 17 tests for which experimental peak displacement values are available (i.e., excluding broken sensor data), a mean value of 0.99 and a coefficient of variation (CV) of 9.3% are achieved for the simulated-to-experimental ratios. Furthermore, the peak displacements of previously damaged specimens are captured very well. For the second and third analyses of the damaged beams (10 tests), the mean ratio and CV of 0.98 and 7.1 % are obtained. The accuracy of the results is particularly notable considering the simple modeling process and fast analysis times. More details on the complete set of simulations may be found in Guner and Vecchio (2012).

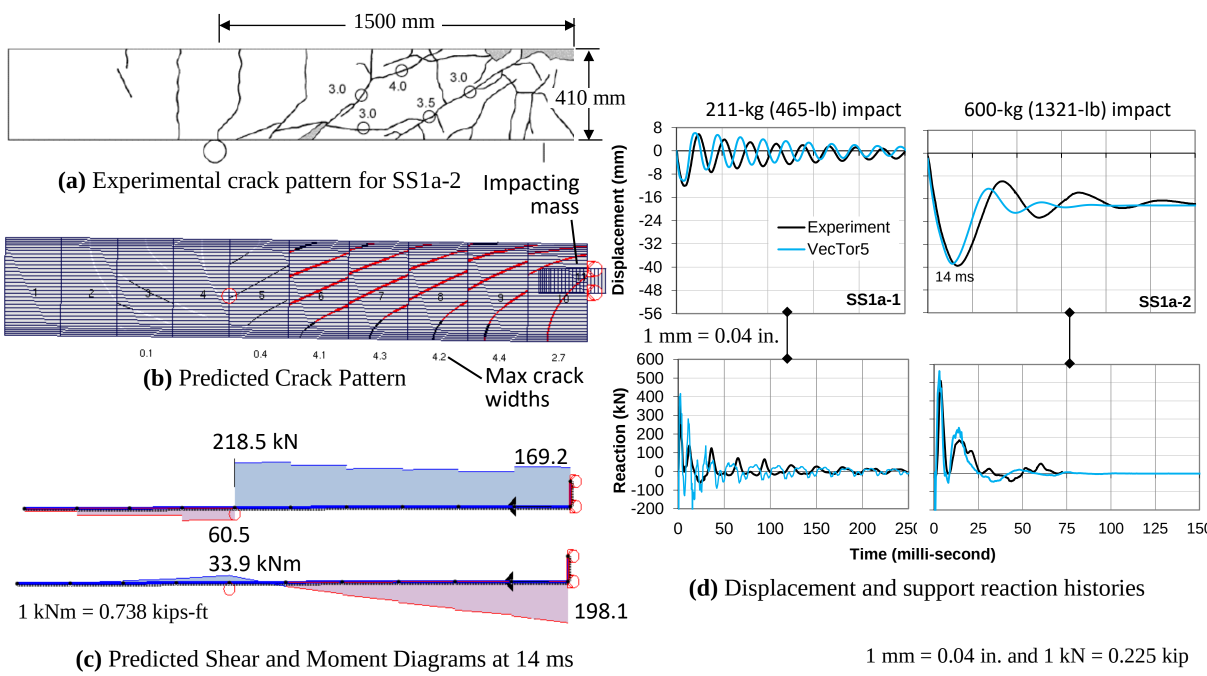

Fig. 12 – Sample impact analysis results for Beam SS1a-1 and SS1a-2 600-kg (1321-lb) impact.

As another example, the blast load analyses performed on doubly reinforced panels, tested in a compressed gas-driven blast load simulator at the Engineer Research and Development Center (ERDC) in Vicksburg, MS, are presented in Fig. 13. The slabs had a thickness of 102 mm (4 in.) and were supported in the longitudinal direction by steel sections, which left a clear span of 1320 mm (52 in.). The panels examined here include double mat reinforcement with either 469-MPa (68-ksi) conventional (NR) or 572-MPa (83-ksi) vanadium reinforcing bars (VR) in combination with 27.6-MPa (4-ksi) (NSC) or 107-MPa (15.5-ksi) (HSC) concrete. More details on the experimental program may be found in Robert and Johnson (2009).

The frame models were created for one-half of the specimens benefiting from the symmetry and include 14 elements. The sectional models uses 34 concrete layers, with a constant layer thickness of 3 mm (0.12 in.) and two discrete steel layers. The midspan displacement responses are calculated reasonably accurately (Fig. 13). The calculated peak reinforcement strains are in the range of 30 milli-strain, and the calculated maximum crack width is approximately 4.5 mm (0.18 in.). Only the maximum crack widths were reported in the experimental study as 4.2 mm (0.17 in.), which agrees well with the calculated responses. The analysis time was in the range of 3 minutes on a notebook computer with a dual-core 1.8 GHz processor. The same panels were modelled in Thiagarajan et al. (2015) with the FEA software LS-DYNA (2006). These models included constant stress, eight-noded hexahedron elements, with two different meshes—namely, 25.4 and 12.7 mm (1 and 0.5 in.)—in combination with two different concrete models—namely, Concrete Damage Model Release 3 (CDMR3) and Winfrith Concrete Model (WCM). The analyses required significant material model input and analysis option selections and conducted as a part of a master’s study by Vasudevan (2012). The analysis time reported was 10 minutes for the 25.4 mm (1 in.) mesh, and 25 minutes for the 12.7 mm (0.5 in.) mesh on a computer with unknown specifications. These times do not include the finite element model preparation and analysis result acquisition times. The response predictions obtained from these models are shown in Fig. 13. The results highlight the challenges with using general-purpose finite element analysis software with many materials model input and analysis option selections. The computed responses are greatly affected by these selections, and it is possible to obtain rather inaccurate results for blind modeling studies when there is no experimental data available.

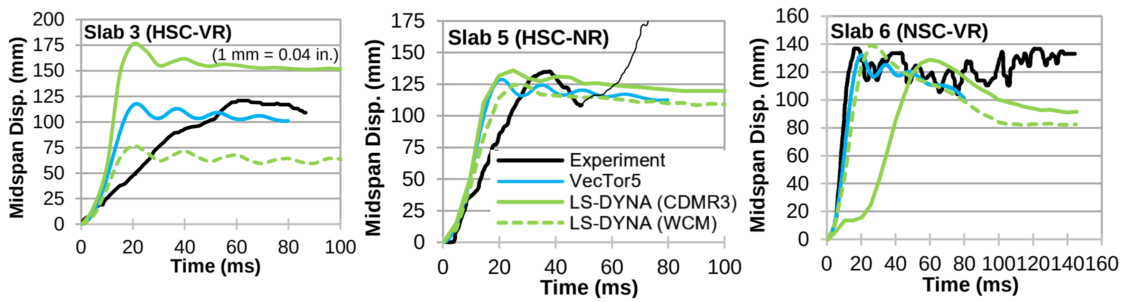

(a) Displacement histories

1 mm = 0.04 in.

(b) Experimental failure modes

Fig. 13 – Sample blast analysis results for doubly-reinforced slabs.

As a seismic load analysis example, a one-story, two-bay frame, subjected to a modified version of the Villa del Mar record of the 1985 Chile earthquake with a peak ground acceleration of 0.79 g, was examined. The frame consists of two well-confined circular outer columns and one poorly confined square center column with 2.5% longitudinal and 0.18% wire transverse reinforcement ratios. The columns support a 1537 mm (5 ft) wide and 343 mm (13.5 in.) deep beam, which represents the transfer beam of a seven-story building. The beam supports piles of steel weights, resulting in a total mass of 30.4 tons (67 kips), including the self-weight of the beam. More details on the experimental program may be found in Elwood and Moehle (2003).

The frame model was created using 68 members as shown in Fig. 14(a). Four member types are used for the sectional models of the top beam, columns, and footing beams; an additional four member types are used for the stiffened joint zone members. In addition to the self-weight and self-mass of the structure, additional masses and gravity loads are applied to the top beam to simulate the steel blocks. The acceleration history data used in the analysis is the one recorded during the test as the shake table output. The Wilson's theta method, with no additional viscous damping and a time-step length of 0.25 ms was used in the analysis. The input accelerogram had time intervals of 10 ms; therefore, each input time step is divided into 40 equal intervals.

The base shear response of the frame is captured accurately with a calculated-to-observed peak shear force ratio of 1.08. Furthermore, the damping of the base shear response shows strong similarities to the experimental response. In the analysis, the first significant cracking occurred at approximately 17.7 seconds when the center column suffered up to 0.8 mm (0.03 in.) wide shear cracks. This time stage marks the first peak in the displacement response, shown with ▲ in Fig. 14(b). At approximately 25.7 seconds, the central column reached its shear capacity at Member 57. At this time stage, shown with ■ in Fig. 14(b), the shear crack widths of the central column reached 1.8 mm (0.07 in.). At approximately 28.8 seconds, the analysis indicated the shear failure of the central column at Member 57 initiated by the fracture of its tie reinforcement [Fig. 14(d)]. This time stage, shown with ♦ in Fig. 14(b), marks the start of significant deterioration of the frame's lateral stiffness and significant redistribution of the axial force from the central to outer columns. The frame exhibited similar behavior in the experiment. The first major shear cracking was observed at the central column at 16.7 seconds; the shear capacity of the central column was reached at 24.9 seconds and the top portion of the center column failed in shear at 29.8 seconds [Fig. 14(e)]. After this failure, significant spalling of the concrete and subsequent buckling of the longitudinal reinforcement at the top portion of the central column was observed. The results demonstrate the large range of performance parameters that may be obtained through a nonlinear time-history analysis.

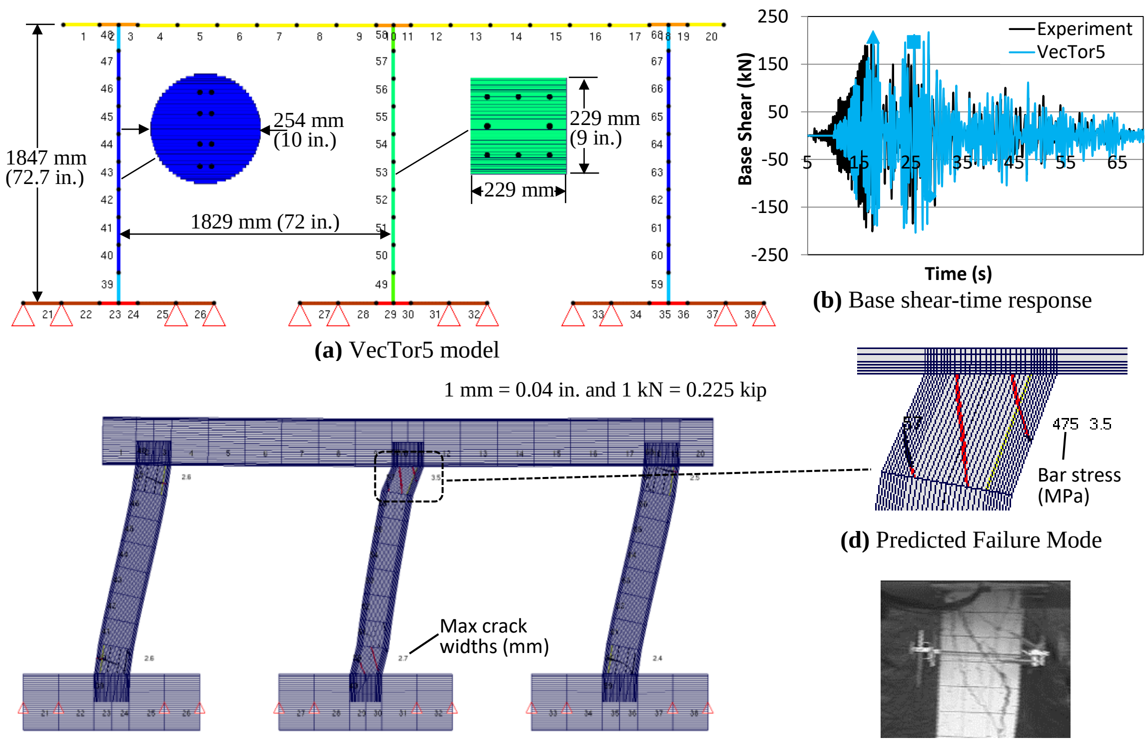

(a) VecTor5 model

(b) Base shear-time response

(c) Predicted condition at 28.8 s

(d) Predicted Failure Mode

(e) Experimental failure mode

Fig. 14 – Sample seismic analysis model and results for a shear-critical frame supporting 30.4 tons of mass.

Summary of Dynamic Analysis Results

The peak displacements obtained from all dynamic time-history analyses are presented in Table 3 in comparison with the experimental results. Considering all 62 dynamically loaded beam, column, slab, and frame specimens, a mean of 0.98 and a coefficient of variation of 15.1% are obtained for the calculated-to-experimental peak displacement ratios. Fourteen of the blast loaded specimens were modelled using the FEA software LS-DYNA (2006) in Thiagarajan et al. (2015) and Thiagarajan and Johnson (2014), either using Concrete Damage Model Release 3 (CDMR3) or Winfrith

Concrete Model (WCM). Using the peak displacement values reported, the mean and COV values were found to be 1.10 and 11% for the CDMR3, and 0.90 and 15% for the WCM for the same 10 slabs. These analyses required significant material model input and analysis option selections conducted as a part of a master's study by Shetye (2013) and Vasudevan (2012). The results highlight the benefits of the developed method with default material models specifically developed for reinforced concrete elements. In addition, stiffnesses, residual deflections, and damage and failure modes were captured accurately. More details on the modeling studies undertaken for these specimens may be found in the references cited in Table 3. The readers are encouraged to model some of these specimens to gauge the accuracy of the modeling method and software that they use.

Table 3 – Comparison of the calculated peak displacements with experimental values for dynamic load conditions.

Impact Loading			Peak displacement (mm)		
		Specimen	VT5	Exp	VT5/Exp
1	**Beams** (Guner and Vecchio 2012)	SS0a-1	11.7	9.3	1.26
2		SS1a-1	10.3	11.9	0.87
3		SS2a-1	10.1	10.5	0.96
4		SS3a-1	10	10.6	0.94
5		SS0b-1	S.F.	S.F.	n/a
6		SS1b-1	37.6	39.2	0.96
7		SS2b-1	37.4	37.6	0.99
8		SS3b-1	37.8	35.1	1.08
9		SS0a-2	S.F.	S.F.	n/a
10		SS1a-2	38.8	39.3	0.99
11		SS2a-2	37.5	38.1	0.98
12		SS3a-2	38.1	36.8	1.04
13		SS1b-2	62.9	76.6	0.82
14		SS2b-2	58.6	61.5	0.95
15		SS3b-2	57.2	54.6	1.05
16		SS1a-3	64.5	n/a	n/a
17		SS2a-3	60.2	56.6	1.06
18		SS3a-3	58.7	57	1.03
19		SS2b-3	32.4	34.3	0.94
20		SS3b-3	28.7	30.4	0.94
				Mean	**0.99**
				CV	**9.3%**

Blast Loading			Peak displacement (mm)		
		Specimen	VT5/Exp	CDMR3/Exp	WCM/Exp
1	**Slabs and Slab Strips** (Guner 2016)	Slab 2	1.13	1.10	0.77
2		Slab 4	1.06	1.00	0.73
3		Slab 6	1.19	1.09	0.67
4		Slab 8	1.08	1.09	0.83
5		Slab 10	1.05	1.11	0.91
6		Slab 12	1	1.08	0.95
7		Slab 1	0.98	0.98	0.98
8		Slab 5	1.01	1.37	1.20
9		Slab 9	0.75	1.03	0.96
10		Slab 11	0.91	1.15	0.96
11		Slab 3	0.97	0.83	0.62
12		Slab 5	0.92	0.86	0.89
13		Slab 6	1.02	1.00	1.06
14		Slab 9	0.64	0.67	0.75
15		CS1-1	1.13		
16		CS1-2	0.99		
17		CS2-1	1		
18		CS2-2	0.94		
19		CS3-1	0.88		
20		CS3-2	0.97		
21		CS3-3	1.01		
22		TX-1	1.42		
23		TX-2	1.29		
24		TX-3	1.09		
		Mean	**1.02**	**1.03**	**0.88**
		CV	**15.2%**	**15.5%**	**17.3%**

Seismic Loading			Peak displacement (mm)		
		Specimen	VT5	Exp	VT5/Exp
1	**Frame and Columns** (Guner and Vecchio 2012)	A1-1	18.85	31.575	0.60
2		A1-2	136	124.37	1.09
3		A1-3	173.2	142.09	1.22
4		A1-4	122.4	107.18	1.14
5		A1-5	154.3	155.65	0.99
6		A1-6	146.9	175.54	0.84
7		A1-7	104.5	98.898	1.06
8		A1-8	145.1	199.62	0.73
9		B1-1	3.641	5.9479	0.61
10		B1-2	13.91	13.321	1.04
11		B1-3	21.85	20.765	1.05
12		B1-4	32.51	37.722	0.86
13		B1-5	85.09	86.817	0.98
14		B1-6	119.2	150.26	0.79
15		B1-7	74.36	78.749	0.94
16		B1-8	127	133.11	0.95
17		B1-9	136.2	128.88	1.06
18		S1	74	89.4	0.83
				Mean	**0.93**
				CV	**18.2%**

	Cummulative
Number of specimens	62
VT5/Exp **Mean**	**0.98**
VT5/Exp **CV**	**15.1%**

1 kN = 0.225 kip

SUMMARY AND CONCLUSIONS

In this study, a frame analysis method incorporating slender, deep, and beam-column joint elements is presented for the nonlinear static and dynamic analysis of reinforced concrete structures. The method aims to combine the simplicity of frame elements with the accuracy and result visualization capabilities of continuum elements. Key results obtained from the studies presented in this paper support the following conclusions:

1. Nonlinear modeling of concrete elements requires comprehensive and fast analysis tools. Pre- and post-processor software is essential in understanding the behavior and failure mode by displaying the sequence of nonlinear events, crack propagation, concrete and reinforcement stresses and strains, and the deflected shapes.
2. The general-purpose finite element analysis software, used to model structures made from many materials including steel, concrete and timber, demands expert knowledge, requires a large number of input parameters, and takes significant modeling and analysis time. The accuracy obtained is highly dependent on the analysis option selections and the material model parameters input.
3. Accurately capturing the behaviour of shear-critical reinforced concrete elements with general-purpose finite element analysis software continues to represent a major challenge.
4. The Disturbed Stress Field Model can successfully be employed to capture the shear-critical behavior under a large range of loading conditions including monotonic, cyclic, and dynamic load cases.
5. The explicit time-step numerical integration method, derived based on the total-load and secant-stiffness-based solution algorithm, exhibits excellent convergence and numerical stability characteristics even in the heavily damaged post-peak stages of the dynamic time-history analyses. The accurate prediction of the post-peak response is essential when determining the ductility, sequence of nonlinear events, and the ultimate failure mode of a frame.
6. The developed analysis method accurately simulated the experimental behaviors of the specimens examined. Peak loads, deflections, stiffnesses, residual deflections, and damage and failure modes (including shear failures) were

captured accurately. Considering all 148 simulations, a mean value of 0.99 and COV of 13.4% were obtained for the calculated-to-observed peak force and displacement ratios.

7. Multiple successive analyses were successfully undertaken for the previously loaded specimens, taking the previous damage into account. For the second and third impact analyses of the damaged beams (10 tests), the mean ratio and CV were 0.98 and 6.9%. For the second and third blast analyses of panels (6 tests), a mean value of 1.05 and COV of 11.2% were obtained.
8. The developed method uses simple models with line elements, and default material models and analysis options. In addition, it requires a fraction of the modeling effort and analysis time demanded by continuum finite element methods.

ACKNOWLEDGMENT

The author would like to thank Dr. Frank J. Vecchio for co-authoring the computer program VecTor5 and his continuous guidance and mentorship over the years. The author also extends his gratitude to Dr. Selcuk Saatci and Dr. Ganesh Thiagarajan for providing the experimental data of the SS beams and blast-loaded slabs, respectively. MS student, Prativa Pathak is acknowledged for her help in preparing Tables 2 and 3.

REFERENCES

Akkaya, Y., Guner, S., and Vecchio, F. J. (2019) "Constitutive Model for the Inelastic Buckling Behavior of Reinforcing Bars," *ACI Structural Journal*, 116(3): 195-204. Retrieved from https://www.utoledo.edu/engineering/faculty/serhan-guner/docs/JP11_Akkaya_et_al_2019.pdf

Angelakos, D.; Bentz, E. C.; and Collins, M. P. (2001) "Effect of Concrete Strength and Minimum Stirrups on Shear Strength of Large Members," *ACI Structural Journal*, 98(3):290-300. Retrieved from https://doi.org/10.14359/10220

Attaalla, S. A.; Agbabian, M. S. (2004) "Performance of Interior Beam-Column Joints Cast from High Strength Concrete under Seismic Loads," *Advances in Structural Engineering*, 7(2):147-57. Retrieved from https://doi.org/10.1260/1369433041211093

Bentz, E. and Collins. M.P. (2001) "Response-2000, Shell-2000, Triax-2000, Membrane-2000 User Manual," Department of Civil Engineering, University of Toronto, Canada. Retrieved from https://www.ut-sim.ca/numerical-simulation.html

Blosser, K., Guner, S., and Vecchio, F. J. (2016) "User's Manual of FormWorks Plus for VecTor5," Online Publication, 29 pp. Retrieved from http://www.utoledo.edu/engineering/faculty/serhan-guner/docs/M3_VT5FWPManual.pdf

Cervenka, V. and Cervenka, J. (2015) "User's Manual for ATENA 2D," Prague, Czech Republic. Retrieved from https://www.cervenka.cz/products/atena/documentation/

Chak, I.N. (2013) "Janus: A Post-Processor for VecTor Analysis Software," MASc Thesis, Department of Civil Engineering, University of Toronto, ON, Canada, 193 pp. Retrieved from http://www.vectoranalysisgroup.com/theses/Chak-MASc(2013).pdf

Clough, R. W. and Penzien, J. (1993) Dynamics of Structures, 2nd Edition, McGraw-Hill, New York, 738 pp.

CSA A23.3 (2024) "Design of Concrete Structures," Canadian Standards Association, Mississauga, ON, Canada, 314 pp.

CSI (2016) "Integrated Software for Structural Analysis and Design User's Manual," Version 19, Computers and Structures, Inc., Berkeley, CA, USA. Retrieved from https://docs.csiamerica.com/manuals/sap2000/CSiRefer.pdf

Dunkman, D. A.; Yousef, A. E. A.; Karve, P. M.; and Williamson, E. B. (2009) "Blast Performance of Prestressed Concrete Panels," Proceedings of the 2009 Structures Congress: Don't Mess with Structural Engineers: Expanding Our Role, pp. 1297-1306. Retrieved from https://doi.org/10.1061/41031(341)142

Duong, K. V.; Sheikh, S. A.; and Vecchio, F. J. (2007) "Seismic Behavior of Shear-Critical Reinforced Concrete Frame: Experimental Investigation." *ACI Structiral Journal*, 104(3): 304–313. Retrieved from vectoranalysisgroup.com/journal_publications/jp61.pdf

Elwood, K. J. and Moehle, J. P. (2003) “Shake Table Tests and Analytical Studies on the Gravity Load Collapse of Reinforced Concrete Frames,” PEER Report 2003/01, University of California, Berkeley, CA, 346 pp. Retrieved from https://peer.berkeley.edu/publications/2003-01

fib Model Code (2010) “*fib* Model Code for Concrete Structures,” Ernst & Sohn, Oct. 2013, 434 pp. Retrieved from https://www.fib-international.org/publications/fib-bulletins/model-code-2010-first-complete-draft,-vol-1-pdf-detail.html

Guner, S. (2008) “Performance Assessment of Shear-Critical Reinforced Concrete Plane Frames,” PhD Dissertation, Department of Civil Engineering, University of Toronto, 429 pp. Retrieved from https://www.utoledo.edu/engineering/faculty/serhan-guner/docs/T1_Guner_PhD_2018.pdf

Guner, S. (2016) “Simplified Modeling of Frame Elements subjected to Blast Loads,” *ACI Structural Journal*, 113(2): 363-372. Retrieved from https://www.utoledo.edu/engineering/faculty/serhan-guner/docs/JP5_Guner_2016.pdf

Guner, S. and Vecchio F. J. (2008) “User’s Manual of VecTor5,” Online publication, 88 pp. Retrieved from https://www.utoledo.edu/engineering/faculty/serhan-guner/docs/M1-VT5Manual-V1-3.pdf

Guner, S. and Vecchio, F. J. (2010a) “Pushover Analysis of Shear-Critical Frames: Formulation,” *ACI Structural Journal*, 107(1): 63-71. Retrieved from http://www.utoledo.edu/engineering/faculty/serhan-guner/docs/JP1_Guner_Vecchio_2010a.pdf

Guner, S. and Vecchio, F. J. (2010b) “Pushover Analysis of Shear-Critical Frames: Verification and Application,” *ACI Structural Journal*, 107(1): 72-81. Retrieved from https://www.utoledo.edu/engineering/faculty/serhan-guner/docs/JP2_Guner_Vecchio_2010b.pdf

Guner, S. and Vecchio, F. J. (2011) “Analysis of Shear-Critical Reinforced Concrete Plane Frame Elements under Cyclic Loading,” *Journal of Structural Engineering*, ASCE, 137(8): 834-843. Retrieved from https://ascelibrary.org/doi/abs/10.1061/%28ASCE%29ST.1943-541X.0000346

Guner, S. and Vecchio, F. J. (2012) “Simplified Method for Nonlinear Dynamic Analysis of Shear-Critical Frames,” *ACI Structural Journal*, 109(5): 727-737. Retrieved from www.utoledo.edu/engineering/faculty/serhan-guner/docs/JP4_Guner_Vecchio_2012.pdf

Hachem, M. M.; Mahin, S. A.; and Moehle, J. P. (2003) “Performance of Circular Reinforced Concrete Bridge Columns under Bidirectional Earthquake Loading,” PEER Report 2003/06, University of California, Berkeley, CA, 452 pp. Retrieved from https://peer.berkeley.edu/publications/2003-06

Hoshikuma, J., Kawashima, K., Nagaya, K., and Taylor, A.W. (1997) “Stress-Strain Model for Confined Reinforced Concrete in Bridge Piers,” *Journal of Structural Engineering*, ASCE, 123(5): 624-633. Retrieved from https://doi.org/10.1061/(ASCE)0733-9445(1997)123:5(624)

Jacques, E. (2011) “Blast Retrofit of Reinforced Concrete Walls and Slabs,” MASc thesis, Department of Civil Engineering, University of Ottawa, Ottawa, ON, Canada, 196 pp. Retrieved from https://ruor.uottawa.ca/items/3af08762-36c3-4da7-9919-df4ea4f7d016

Kent, D. C. and Park, R. (1971) “Flexural Members with Confined Concrete,” *ASCE Journal of the Structural Division*, 97(7): 1341-1360. Retrieved from https://doi.org/10.1061/JSDEAG.0002957

Kupfer, H., Hilsdorf, H.K., and Rusch, H. (1969) “Behavior of Concrete under Biaxial Stress,” *ACI Journal*, 87(2): 656-666. Retrieved from https://doi.org/10.14359/7388

Liu, J. and Mihaylov, B. I. (2018) “Macroelement for Complete Shear Behavior of Continuous Deep Beams,” *ACI Structural Journal*, 115(4): 1089-1099. Retrieved from https://doi.org/10.14359/51702047

Liu, J.; Guner, S.; and Mihaylov, B. (2019) “Mixed-Type Modeling of Structures with Slender and Deep Beam Elements” *ACI Structural Journal*, 116(4): 253-264. Retrieved from https://www.utoledo.edu/engineering/faculty/serhan-guner/docs/JP11_Liu_et_al_2019.pdf

Loya, A. S.; Lourenço, D. D. S.; Guner, S.; and Vecchio, F. J. (2017) “User’s Manual of Janus for VecTor5,” Online Publication, 28 pp. Retrieved from http://www.utoledo.edu/engineering/faculty/serhan-guner/docs/M2_VT5JanusManual_V2.0.pdf

LS-DYNA (2006) “Theory Manual,” compiled by John O. Hallquist, Livermore Software Technology Corporation, Livermore, CA. Retrieved from https://ftp.lstc.com/anonymous/outgoing/jday/manuals/ls-dyna_theory_manual_2006.pdf

Malvar, L. J. (1988) “Review of Static and Dynamic Properties of Steel Reinforcing Bars,” *ACI Materials Journal*, Vol. 95, No. 5, pp. 609-614. Retrieved from https://doi.org/10.14359/403

Mander, J. B.; Priestley, M. J. N.; and Park. R. (1988) “Theoretical Stress-Strain Model for Confined Concrete,” *ASCE Journal of Structural Engineering*, 114(8): 1804-1826. Retrieved from https://doi.org/10.1061/(ASCE)0733-9445(1988)114:8(1804)

Mihaylov, B. I.; Hunt, B.; Bentz, E. C.; and Collins, M. P. (2015) “Three-Parameter Kinematic Theory for Shear Behavior of Continuous Deep Beams,” *ACI Structural Journal*, 112(1), pp. 47-57. Retrieved from https://doi.org/10.14359/51687180

Mihaylov, B. I.; Bentz, E. C.; and Collins, M. P., “Behavior of Large Deep Beams Subjected to Monotonic and Reversed Cyclic Shear,” *ACI Structural Journal*, 107(6): 726-734.

Newmark, N. M. (1959) “A Method of Computation for Structural Dynamics,” *Journal of the Engineering Mechanics Division ASCE*, 85(3): 67-94. Retrieved from https://doi.org/10.1061/JMCEA3.0000098

Noguchi, H. and Kashiwazaki, T. (1992) “Experimental Studies on Shear Performances of RC Interior Beam-Column Joints,” 10th World Conf. on Earthquake Engineering, Madrid, Spain, 3163-3168. Retrieved from iitk.ac.in/nicee/wcee/article/10_vol6_3163.pdf

Oesterle, R. G.; Fiorato, A. E.; Johal, L. S.; Carpenter, J. E.; Russell, H. G.; and Corley, W. G. (1976). “Earthquake Resistant Structural Walls—Tests of Isolated Walls.” Construction Technology Laboratories, Portland Cement Association, Skokie, IL, 315 pp. Retrieved from https://datacenterhub.org/app/site/collections/shear-wall/pub/Oesterle_1979.pdf

Palermo, D. and Vecchio, F. J. (2004) “Compression Field Modeling of Reinforced Concrete Subjected to Reversed Loading: Verification,” *ACI Structural Journal*, 101(2): 155-164. Retrieved from http://vectoranalysisgroup.com/journal_publications/jp50.pdf

Pan, Z.; Guner, S.; and Vecchio, F.J. (2017) “Modeling of Interior Beam-Column Joints for Nonlinear Analysis of Reinforced Concrete Frames,” *Engineering Structures*, 142: 182-191. Retrieved from https://doi.org/10.1016/j.engstruct.2017.03.066

Park R. and Dai, R. . (1988) “A Comparison of the Behavior of Reinforced Concrete Beam-Column Joints Designed for Ductility and Limited Ductility,” Bulletin of the New Zealand Society for Earthquake Engineering, 21(4):255–78. Retrieved from https://doi.org/10.5459/bnzsee.21.4.255-278

Peng, C. and Guner, S. (2018) "Direct Displacement-Based Seismic Assessment of Concrete Frames Using Nonlinear Pushover Analysis," *Computers and Concrete*, 21(4): 355-365. Retrieved from https://www.utoledo.edu/engineering/faculty/serhan-guner/docs/JP8_Peng_Guner_2018.pdf

Popovics, S. (1973) “A Numerical Approach to the Complete Stress-Strain Curve of Concrete,” *Cement and Concrete Research*, 3(5): 583-599. Retrieved from http://vectoranalysisgroup.com/journal_publications/jp50.pdf

Rayleigh, Lord (1877) Theory of Sound, V.1, Dover Publications (1945), Mineola, NY, 504 pp.

Robert, S. D. and Johnson, C. F. (2009) “Blast Response of Conventional and High Performance Reinforced Concrete Panels,” Proceedings of the 2009 Structures Congress: Don’t Mess with Structural Engineers: Expanding Our Role, Austin, TX, pp. 1142-1150. Retrieved from https://doi.org/10.1061/41031(341)126

Saatci, S. and Vecchio, F. J. (2009a) “Effects of Shear Mechanisms on Impact Behavior of Reinforced Concrete Beams,” *ACI Structural Journal*, 106(1): 78-86. Retrieved from http://www.vectoranalysisgroup.com/journal_publications/jp65.pdf

Saatci, S. and Vecchio, F. J. (2009b) “Nonlinear Finite Element Modeling of Reinforced Concrete Structures under Impact Loads,” *ACI Structural Journal*, 106(5): 717-725. Retrieved from http://www.vectoranalysisgroup.com/journal_publications/jp67.pdf

Sadeghian, V. (2012) “Formworks-Plus: Improved Pre-Processor for Vector Analysis Software,” MASc Thesis, Department of Civil Engineering, University of Toronto, Canada, ON, Canada, 147 pp. Retrieved from http://www.vectoranalysisgroup.com/theses/Sadeghian-MASc(2012).pdf

Salamy, M. R.; Kobayashi, H.; and Unjoh, S. (2005) “Experimental and Analytical Study on RC Deep Beams,” *Asian Journal of Civil Engineering*, 6(5): 409-421.

Seckin, M. (1981) “Hysteretic Behaviour of Cast-in-Place Exterior Beam-Column-Slab Subassemblies,” PhD Dissertation, Department of Civil Engineering, University of Toronto, ON, Canada, 236 pp. Retrieved from https://www.utoledo.edu/engineering/faculty/serhan-guner/docs/T1_Guner_PhD_2018.pdf

Shetye, G. A. (2013) “Finite Element Analysis and Experimental Validation of Reinforced Concrete Single-Mat Slabs Subjected to Blast Loads,” MSc thesis, Department of Civil Engineering, University of Missouri-Kansas City, Kansas City, MO, 155 pp. https://mospace.umsystem.edu/xmlui/handle/10355/35494

Shiohara, H. and Kusuhara, F. (2006). “Benchmark Test for Validation of Mathematical Models for Non-linear and Cyclic Behavior of R/C Beam-column Joints.” http://www.rcs.arch.t.u-tokyo.ac.jp/shiohara/benchmark/test_report.pdf, 126.

Tanimura, Y. and Sato, T. (2005) “Evaluation of Shear Strength of Deep Beams with Stirrups,” Quarterly Report of RTRI, 46(1): 53-58. Retrieved from https://doi.org/10.2219/rtriqr.46.53

Thiagarajan, G. and Johnson, C. F. (2014) “Experimental Behavior of Reinforced Concrete Slabs Subjected to Shock Loading,” *ACI Structural Journal*, 111(6): 1407-1417. Retrieved from https://doi.org/10.14359/51686970

Thiagarajan, G.; Kadambi, A. V.; Robert, S.; and Johnson, C. F. (2015) “Experimental and Finite Element Analysis of Doubly Reinforced Concrete Slabs Subjected to Blast Loads,” *International Journal of Impact Engineering*, 75:162-173. Retrieved from https://doi.org/10.1016/j.ijimpeng.2014.07.018

Vasudevan, A. K. (2012) “Finite Element Analysis and Experimental Comparison of Doubly Reinforced Concrete Slabs Subjected to Blast Loads,” MSc thesis, Department of Civil Engineering, University of Missouri-Kansas City, Kansas City, MO, 74 pp. Retrieved from https://mospace.umsystem.edu/xmlui/handle/10355/14606

Vecchio F. J. (1999) “Towards Cyclic Load Modeling of Reinforced Concrete,” *ACI Structural Journal*, 96(2): 193-202. Retrieved from http://www.vectoranalysisgroup.com/journal_publications/jp29.pdf

Vecchio, F. J. (2000) “Disturbed Stress Field Model for Reinforced Concrete: Formulation,” *Journal of Structural Engineering*, 126(6): 1070-1077. Retrieved from http://www.vectoranalysisgroup.com/journal_publications/jp34.pdf

Vecchio, F. J. and Balopoulou, S. (1990) “On the Nonlinear Behaviour of Reinforced Concrete Frames,” *Canadian Journal of Civil Engineering*, V17(5): 698-704. Retrieved from vectoranalysisgroup.com/journal_publications/jp12.pdf

Vecchio, F. J. and Collins, M. P. (1986) “The Modified Compression-Field Theory for Reinforced Concrete Elements Subjected to Shear,” *ACI Journal*, 83(2): 219-231. Retrieved from http://www.vectoranalysisgroup.com/journal_publications/jp2.pdf

Vecchio, F. J. and Emara, M. B. (1992) “Shear Deformations in Reinforced Concrete Frames,” *ACI Structural Journal*,” 89(1): 46-56. Retrieved from http://vectoranalysisgroup.com/journal_publications/jp16.pdf

Vecchio, F. J. and Shim, W. (2004) “Experimental and Analytical Reexamination of Classic Concrete Beam Tests,” *Journal of Structural Engineering*, ASCE, 130(3): 460-469. Retrieved from http://vectoranalysisgroup.com/journal_publications/jp49.pdf

VecTor5 (2019) “A Nonlinear Finite Element Analysis Program for Two-Dimensional Reinforced Concrete Frame Structures,” Computer software, VecTor Analysis Group (VTAG). Retrieved from http://www.vectoranalysisgroup.com

Walker, S.G. (2001) “Seismic Performance of Existing Reinforced Concrete Beam-Column Joints,” MS thesis. Washington: University of Washington, Seattle, 308 pp.

Wilson, E. L.; Farhoomand, I.; and Bathe K. J. (1973) “Nonlinear Dynamic Analysis of Complex Structures,” *Earthquake Engineering and Structural Dynamics*,1(3): 241-252. Retrieved from http://web.mit.edu/kjb/www/Publications_Prior_to_1998/Nonlinear_Dynamic_Analysis_of_Complex_Structures.pdf

Wong, P. S.; Vecchio, F. J.; and Trommels, H. (2013) “VecTor2 and FormWorks User’s Manual,” Technical Report, VecTor Analysis Group (VTAG), 347 pp. Retrieved from http://www.vectoranalysisgroup.com/user_manuals/manual1.pdf.

Wu, C. L.; Kuo, W. W.; Yang, Y. S.; Hwang, S. J.; Elwood, K. J.; Loh, C. H.; and Moehle, J. P. (2008) “Collapse of a Nonductile Concrete Frame: Shaking Table Tests,” *Earthquake Engineering and Structural Dynamics*, 38(2): 205-224. Retrieved from https://doi.org/10.1002/eqe.853

Xue, W.C.; Cheng, B.; Zheng, R.G.; Li, L.; and Li, J. (2011) “Seismic Performance of Nonprestressed and Prestressed HPC Frames under Low Reversed Cyclic Loading,” *Journal Structural Engineering*, ASCE, 137(11): 1254-1262. Retrieved from https://doi.org/10.1061/(ASCE)ST.1943-541X.0000367

Yavari, S.; Elwood, K.J.; Wu, C.L.; Lin, S.H.; Hwang, S.J; and Moehle, J.P. (2013) “Shaking Table Tests on Reinforced Concrete Frames without Seismic Detailing,” *ACI Structural Journal*, 110(6): 1001-1011. Retrieved from https://doi.org/10.14359/51686155